

Optimizing PatchCore for Few/many-shot Anomaly Detection

João Santos, Triet Tran, Oliver Rippel
 Scortex
 22 Rue Berbier du Mets
 jsantos@scortex.io

Abstract

Few-shot anomaly detection (AD) is an emerging sub-field of general AD, and tries to distinguish between normal and anomalous data using only few selected samples. While newly proposed few-shot AD methods do compare against pre-existing algorithms developed for the full-shot domain as baselines, they do not dedicatedly optimize them for the few-shot setting. It thus remains unclear if the performance of such pre-existing algorithms can be further improved. We address said question in this work. Specifically, we present a study on the AD/anomaly segmentation (AS) performance of PatchCore, the current state-of-the-art full-shot AD/AS algorithm, in both the few-shot and the many-shot settings. We hypothesize that further performance improvements can be realized by (I) optimizing its various hyperparameters, and by (II) transferring techniques known to improve few-shot supervised learning to the AD domain. Exhaustive experiments on the public VisA and MVTEC AD datasets reveal that (I) significant performance improvements can be realized by optimizing hyperparameters such as the underlying feature extractor, and that (II) image-level augmentations can, but are not guaranteed, to improve performance. Based on these findings, we achieve a new state of the art in few-shot AD on VisA (Fig. 1), further demonstrating the merit of adapting pre-existing AD/AS methods to the few-shot setting¹. Last, we identify the investigation of feature extractors with a strong inductive bias as a potential future research direction for (few-shot) AD/AS.

1. Introduction

Image anomaly detection (AD) and anomaly segmentation (AS) are respectively tasked with identifying abnormal images, and with localizing the abnormal patterns inside said images [13, 37, 44]. Here, an anomaly is defined simply as being a deviation from a pre-defined/learned concept of nor-

¹We also obtained first place in the few-shot AD track of the VAND challenge at CVPR 2023 with this approach, see <https://sites.google.com/view/vand-cvpr23/challenge>.

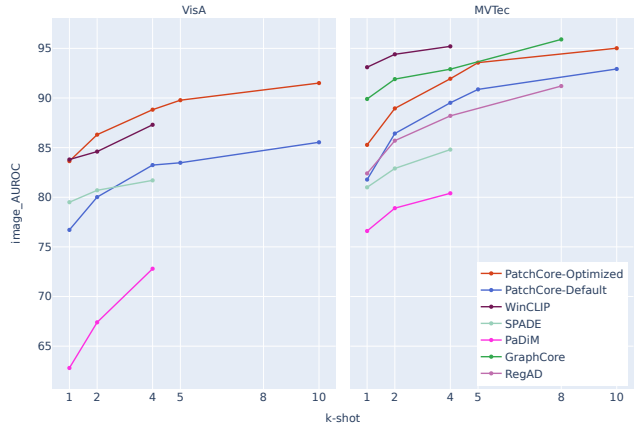


Figure 1. Optimizing the hyperparameters of existing full-shot AD methods such as PatchCore [42] boosts their few-shot performance and furthermore yields state-of-the-art AD results on VisA [63].

mality [13, 37, 44]. AD/AS play a crucial role in domains such as medical image analysis, video surveillance, or automated visual inspection (AVI), where anomalies correspond to diseases, threats, and defects, respectively [9, 33, 45].

Due to the limited availability of anomalous data, current AD/AS methods are typically trained in a one-class fashion, using (large amounts of) normal data only [15, 18, 40, 42–44, 56, 59]. They furthermore tend to exploit features from models pre-trained on large corpora of (natural) images such as ImageNet [19], assuming that the target AD domain will be close enough to the domain used for pre-training [15, 18, 40, 42, 43, 60]. Some of these methods have shown outstanding performance on the full-shot setting, i.e. when training with >100 normal images. As a consequence, popular datasets generally used for benchmarking developed methods are practically solved. For example, the state-of-the-art method PatchCore [42] obtains 99.6% area under the receiver operating characteristic (ROC) curve (ROC) on MVTEC AD [7, 9], a dataset focused on AVI.

As a consequence to this saturation, the few-shot as well as the many-shot settings have been proposed recently, which aim to solve the AD/AS task with less normal data

[24, 42, 43, 46]. While no consensus has been established yet on where to draw the exact line between few-shot, many-shot, and full-shot AD/AS, literature typically considers ≤ 10 images to be few-shot, and ≥ 100 images to be full-shot [3, 24, 27, 43, 46]. Performing well in both the few and the many-shot setting is furthermore essential for domains where the acquisition of labeled normal data is very resource-intensive, such as the medical or industrial domains [42, 45]. In both settings, performances comparable to the full-shot regime have furthermore not yet been achieved [3, 24, 27, 43, 46, 53]. However, current efforts focus on developing novel algorithms for the few and the many-shot settings, rather than adapting/optimizing existing methods [3, 24, 27, 53].

In this work, we focus on improving existing AD/AS algorithms in both the few-shot and the many-shot setting. We argue that the hyperparameters of current AD/AS methods are overfit to the full-shot setting, and that thus further performance gains can be realized by optimizing them. We show this to be true for PatchCore [42], the current state-of-the-art full-shot AD/AS algorithm. We moreover investigate whether data augmentation techniques, which are known to improve performance for supervised learning in the limited data regime, are also beneficial for few/many-shot AD/AS. Specifically, we show through extensive experiments, that:

- The trend that architectures with stronger ImageNet performance are also better for AD/AS [40] is not confirmed in the few and many-shot AD regimes.
- Increasing the inductive bias of convolutional neural networks (CNNs) by enforcing translation equivariance improves performance, revealing a potential avenue for future research.
- Image-level augmentations can improve few-shot performance overall, but must be tuned carefully to do so.
- Greedy coreset subsampling neither increases nor decrease performance, while simultaneously lowering the size of the memory bank significantly.
- Combining all of this leads to a new state of the art in few-shot AD on the challenging VisA dataset [63] (Fig. 1), demonstrating the merit of adapting pre-existing AD/AS methods to the few/many-shot settings. This is further supported by the fact that we obtained first place in the few-shot AD track of the VAND challenge at CVPR 2023 with this approach.

To ensure reproducibility, we provide the full code with detailed instructions at <https://github.com/scortexio/patchcore-few-shot/>.

2. Related Work

2.1. AD in the Few/many-shot Regime

Currently, only few works propose methods to specifically tackle the few/many-shot AD/AS problem [11, 14, 24, 27, 43, 53]. Similarly to the full-shot regime, proposed methods generally use a pre-trained feature extractor to extract relevant features from the input image data [24, 27, 43]. However, there also exist methods that rely on learning features from scratch. For example, authors in [53] propose learning visual, isometric invariant features with graph neural networks to handle the low amount of training data inherent to the few-shot setting. Alternatively, vision-language based methods have been proposed recently [11, 14, 27], which leverage pre-existing domain knowledge via language prompting and have shown impressive results both on the zero-shot and few-shot settings. Vision-language-based methods are, however, quite expensive from a computational point of view, and thus not easily applicable under hardware/time constraints, present e.g. in AVI. They moreover require careful prompt engineering to work, often leveraging pre-existing domain knowledge to maximize performances.

While recently developed few/many-shot AD/AS methods compare among one another and report results of pre-existing full-shot methods applied to the few/many-shot setting as baselines [27, 53], none of them dedicatedly optimize the baselines to the few/many-shot setting. In other domains however, this was shown to be important, since baselines often demonstrated competitive performances when optimized to the target application/domain [25, 34].

A baseline suitable for such optimizations is PatchCore [42], a state-of-the-art deep learning-based algorithm for image AD/AS. PatchCore stores locally aware patch features extracted from normal training images into a memory bank. This memory bank represents a hyper-dimensional space of “normality”. During inference, each patch from the inferred image is compared with all patches in the memory bank to obtain an anomaly score. This score is expected to be higher for anomalous patches compared to normal ones. PatchCore, intended to be used in the full-shot AD regime, has been previously tested on the few/many-shot settings and has shown promising preliminary results here [27, 42, 53, 54]. However note that, as of now, PatchCore has not been dedicatedly optimized for these settings. At most, authors of GraphCore [53] have combined PatchCore with image-level data augmentations to motivate their method.

2.2. Transferring Techniques from Supervised Few-shot Learning to Anomaly Detection

Techniques developed to improve supervised few-shot classification and/or transfer learning performance com-

prise data augmentation [16, 36], improved feature extractors [20, 30, 48], and training on larger input sizes [42, 47, 48], all of which have not been explored exhaustively in the few/many-shot AD settings so far. Moreover, the limited previous work that explores these techniques in context of few/many-shot AD/AS [21, 54, 61] has focused their evaluations on simple datasets such as MVTec AD [7, 9], rather than on more comprehensive and challenging datasets like VisA [63]. The original authors of PatchCore [42] furthermore analysed the performance of different resolutions and feature extractors, but only on the full-shot regime and only using MVTec AD [42]. Finally, authors in [22] performed a comprehensive analysis on the influence of feature extractors, layer selection and input resolutions on different AD/AS algorithms, but also limit their work to the full-shot AD setting. They further evaluate only on the MVTec AD dataset, and conducted their work concurrent to the study presented here.

Modifications like the ones mentioned above can be easily plugged into PatchCore, as detailed in the following.

3. Optimizing PatchCore for Few/many-shot Anomaly Detection

3.1. Better Feature Extractors

Since PatchCore is essentially a k -nearest neighbor (NN) search in intermediate feature representations of pre-trained feature extractors, performance gains should be possible by optimizing the used feature extractor.

Regarding feature extractors and their transferability, it has been shown that model architectures with better classification performance on large-scale and varied datasets, such as ImageNet [19], also achieve better transfer learning performance on downstream tasks [28]. Note that literature is currently inconclusive on whether this trend also holds for methods that leverage pre-trained feature extractors for AD [22, 40]. Moreover, models with a weak inductive bias, e.g. transformer-based architectures, have been introduced in the computer vision domain recently [20]. These models have achieved state-of-the-art results, both on the full-shot [20], but also on the few-shot supervised learning settings [23]. From this, it can be hypothesized that less-constrained models would also perform well in the few/many-shot AD/AS setting.

Contrary to this, a stronger inductive bias is generally assumed to require less data to perform well [6, 26], since some assumptions regarding the underlying data are already incorporated into the model itself. Those assumptions thus do not need to be learned from the data by the model. We explore more constrained models in our work, as we believe them to be crucial for performing well in the few-shot setting, where the low amount of training data increases the risk of mismatch between training and real data distribu-

tions. Specifically, we investigate how much anti-aliasing, a technique used to restore the translation equivariance of CNNs [62], will affect few/many-shot AD/AS performance.

3.2. Increased Resolution

Typically, there is a trade-off between the computational cost and the size of the input image in the sense that a higher input resolution allows us to capture more fine-grained details at the cost of a bigger computational cost, and potentially more unstable training [49].

In the full-shot AD regime, increasing the resolution of the input images to extract finer-grained features has shown to boost AD/AS performance [42]. While there is additional research needed to identify the underlying mechanisms here, initial work hypothesizes that the detectability of defects is determined by the combination of their size and the effective receptive field sizes of the pre-trained feature extractor’s layers [22]. Integrating this into PatchCore is straightforward for CNNs-based feature extractors, and possible with tricks for transformer-based networks [20, 29].

3.3. Data Augmentation

Data augmentation tries to improve the generalization of models by adding sensible variability to the training dataset [16, 36]. It has been extensively used in the supervised learning domain on different data types, ranging from images, text to audio [5, 36, 51]. Some studies have also looked into performing a search for the best augmentation setup for each dataset [16]. Related work has further shown for specific data augmentations such as rotations or translations to improve AD performance [21, 54], and we therefore include them in the considered/assessed augmentations.

Conversely, other techniques have been developed that augment the intermediate feature representations of the model directly [35, 50], instead of modifying the input image space. These variations are designed to induce semantically meaningful changes to the feature space, and thus require assumptions about the semantics of the feature space (e.g. target classes should follow Gaussian distributions in them [50]). Conceptually, feature-based augmentations are much more elegant than image-based augmentations, since they require less expertise in the source domain, and the same augmentations could potentially be applied across domains. While we did investigate feature-based augmentations, we did not succeed. We thus leave their study to future work.

Both image-level and feature-level augmentations can be easily integrated into PatchCore during the construction of the k -NN memory bank (i.e. by augmenting either input images prior to feature extraction or by augmenting the extracted feature representations).

3.4. Coreset Subsampling

Coreset selection is a technique used in machine learning and data analysis to identify a representative subset of data that maintains the same topology as the full dataset [1, 32]. PatchCore uses this technique to significantly reduce its memory bank size, such that the inference time and memory usage can be kept low when we have a higher amount of training images, input resolution, or embedding dimensionality.

PatchCore was shown to work well in conjunction with a greedy coreset construction, which can also slightly improve performance in the full-shot AD regime [42]. In the few-shot regime this technique has not been extensively explored, possibly since the memory bank is already small here. We hypothesize that this technique may also bring a benefit to the few-shot/many-shot AD settings if used in conjunction with data augmentation techniques, and thus investigate its use in this work.

4. Experiments and Results

4.1. General Setup

We select PatchCore for optimization due to its outstanding full-shot AD/AS performance combined with its simplicity, and evaluate on MVTec AD [7, 9] and VisA [63] to evaluate performances. MVTec AD [7, 9] and VisA [63] constitute the two biggest publicly available AD/AS datasets dealing with AVI. In total, they comprise 22 objects and 5 texture categories, with >2400 anomalous and >13 500 normal images.

We evaluate in the few-shot (1, 5 and 10) and in the many-shot (25 and 50) settings, and draw the training samples from each respective category’s training set. For each object category, every k-shot was run with randomly chosen training seeds/images for a total of 5 times, and the same seeds/images are used across all experiments to ensure direct comparability. We furthermore used the PatchCore implementation from the anomalib library as the base [2], and made modifications according to our experiments. We used the default configuration of anomalib, but fixed the number of NNs used for calculating the anomaly score to 1. We observed a small improvement here compared to the reweighting of scores from multiple neighbors proposed by PatchCore, but did not ablate on this.

4.2. Metrics

To evaluate image-wise AD performance, we computed the AUROC [38]. We followed [63] and computed the area under the precision-recall (PR) curve (PR) [17] to evaluate AS performance due to the extreme class imbalance on the pixel-level. Finally, to evaluate the joint AD/AS performance, we used the Harmonic mean of image-AUROC

and pixel-AUPR (HPROC), arguing that consistent performance across both AD/AS tasks is important. We have not used the F1-max score as done in previous work [27, 63], since the PR curve, and consequently the F1-max score derived from it, is overestimated when we have more anomalous than normal samples. This is the case for the test sets of both MVTec AD and VisA at the image-level. To analyse the overall performance in the few/many-shot domains, we propose to plot the HPROC values vs. the respective k-shots, and compute the area under this HPROC-k-shot curve (AUHPROC).

4.3. Influence of Dataset, Feature Extractor and Input Resolution

We start by analysing the influence of dataset, employed feature extractors, and input resolution on AD/AS performances in the few and many-shot regimes. To keep the computational cost at a reasonable level, we perform neither coreset subsampling nor image-level augmentations.

Feature extractors: We assess a set of different feature extractors. For each feature extractor, we do not ablate over the layer selection used, but instead we follow previous work by using intermediate to later layers of the network [22, 42]. We note, however, that jointly optimizing this might yield further performance improvements [22]. Concretely, we use the following combination of feature extractors, original input resolution and layer selection²:

- WideResNet50 [58] (224x224, layers 2 and 3), since it is the baseline used by the majority of AD/AS methods and the default backbone used in PatchCore.
- EfficientNetB4 [48] (380x380, layers 4, 6 and 7) and ConvNext Small/Base [30] (384x384, layers stages.2.blocks.10 and stages.2.blocks.20), to test if better ImageNet performance, which correlates with better transfer learning performance (i.e. more universal feature descriptors), also correlates with better few-shot AD/AS performance. In addition, two ConvNext variants are used to investigate the influence of complexity [18, 41].
- Anti-aliased WideResNet50 [62] (224x224, layers 2 and 3), in order to see if a stronger inductive bias is useful for few/many-shot AD/AS.

Input size ranges: We benchmarked each feature extractor on a range of scales corresponding to 0.5x, 1x, 1.5x and 2x the original input resolution of each model. The assumption here is that higher resolutions increase performance similar as for supervised learning, as we remove less information when downscaling. The 0.5x scale is used to further verify said assumption.

²For complete details please check the code available at <https://github.com/scortexio/patchcore-few-shot/>

Table 1. Performance comparison between MVTEC AD and VisA on few-shot and many-shot regimes. We report the mean and standard deviation of category-wise AUHPROC values computed after averaging over seed/runs.

dataset	AUHPROC			
	few-shot		many-shot	
	mean	std	mean	std
MVTec AD	58.8	18.0	59.3	17.9
VisA	42.6	22.7	43.1	22.9

Results: In order to better understand each of the previous factors, we present the respective performances obtained after marginalizing over the other two parameters.

To analyse the influence of the dataset on the AD/AS performance, we report the mean and standard deviation of category-wise AUHPROC values computed over the few/many-shot settings after averaging over the 5 seeds.

Table 1 shows that, on average, the performance on MVTEC AD is higher than on VisA in both few and many-shot settings. Moreover, the performance on the categories contained in VisA varies more than the performance on the categories contained in MVTEC AD. Overall, this seems to indicate that, across all feature extractors and scales, the VisA dataset is more challenging than MVTEC AD also in the few/many-shot settings. We hypothesize the defect size to be one of the key differentiators between MVTEC AD and VisA, and report the distribution of defect sizes in Appendix A.1. Therefore, future research in few/many-shot AD/AS should focus on more challenging datasets such as VisA or MVTEC LOCO AD [8], rather than evaluating solely on MVTEC AD.

To analyse the effect of the scale on performance, we plot in Fig. 2 the HPROC-k-shot curve for different input scales, averaged over feature extractors, datasets and seeds/runs. An increase in scale generally helps across datasets and feature extractors not only in the full-shot setting as indicated in [42], but also in the few/many-shot settings. Furthermore, it would be interesting to see if the underlying reasons for the performance improvements are truly just that an increase in scale effectively “shifts” the detectability of the defects to be more in the selected layers by modulating the effective receptive field size, as proposed recently [22]. This hypothesis moreover runs counter to the intuition that later layers of a CNN/model encode more semantically abstract features compared to earlier layers [57]. We believe that performing a fundamental validation of said hypothesis, for both semantic/logical as well as structural/textural anomaly types [8, 44], is an interesting avenue of future work.

Finally, to assess the performance of different feature

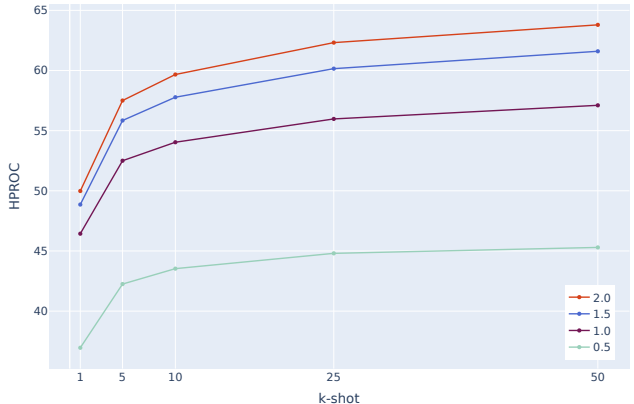


Figure 2. HPROC across k-shots for different input scales, averaged over feature extractors, datasets and seeds/runs.

Table 2. Performance comparison between different backbones at different input scales. We report mean and standard deviation of category-wise AUHPROC generated after averaging over seed-s/runs. Best/second best value per scale are boldfaced/underlined respectively. Abbreviations: AA = Anti-aliased WideResNet50, WRN = WideResNet50, CN-B = ConvNext Base, CN-S = ConvNext Small, ENB4 = EfficientNetB4.

	AUHPROC							
	0.5x		1.0x		1.5x		2.0x	
	mean	std	mean	std	mean	std	mean	std
AA	44.1	29.5	57.9	26.8	63.1	22.1	66.2	18.2
WRN	43.5	29.1	<u>56.6</u>	25.8	<u>62.0</u>	21.9	<u>64.9</u>	19.1
CN-B	46.6	<u>26.3</u>	56.1	<u>21.2</u>	59.5	<u>19.1</u>	60.5	<u>17.1</u>
CN-S	<u>46.3</u>	24.6	54.9	19.6	57.4	17.4	58.3	15.3
ENB4	40.9	28.5	51.5	25.5	55.3	22.5	57.6	20.3

extractors, we compute the AUHPROC category-wise after averaging over the 5 seeds. We then compute mean as well as standard deviation of category-wise AUHPROC for each scale/feature extractor combination. HPROC vs. k-shot curves aggregated over all scales are moreover reported in Appendix A.2.3. Table 2 shows that Anti-aliased WideResNet50 performs best on average compared to the other backbones, followed by the WideResNet50. However, high standard deviations are observed for both versions of the WideResNet50 at lower input scales, and ConvNext models seem to be more consistent across shots and scales overall. Last, the EfficientNetB4 model is neither as capable nor as consistent as any other model that was evaluated. While all assessed feature extractors benefit from an increase in input scale, the realized performance improvement varies across feature extractors. For example, the WideResNet50 improves average AUHPROC by 8.3 while reducing standard deviation by 11.3 when increasing input

scale from 1x to 2x, whereas ConvNext Base improves average AUHPROC only by 4.4 while reducing standard deviation by 4.1. We thus hypothesize that additional variation was incurred for WideResNet-type models by the combination of their low initial input resolution and small defect sizes (see also Appendix A.2.1).

Overall, results presented here do not confirm the positive correlation between ImageNet performance and transfer learning performance [28] for few/many-shot AD/AS, as one would expect ConvNext to be best performing then, followed by EfficientNet. Instead, both WideResNet50 and its anti-aliased version outperform both ConvNext and EfficientNet. Moreover, it can be seen that the "best" feature extractor is different per assessed category (see Appendix A.2.2), which is in line with related work [22]. Furthermore, models of medium complexity remain sufficient for few/many-shot AD/AS performance, since both versions of ConvNext perform comparably. In all, the question "What makes a good feature extractor for (few/many-shot) AD/AS?" therefore still remains unanswered at large.

Our experiments indicate, however, that more constrained feature extractors might be a valid avenue of future research, as the anti-aliased feature extractor outperformed all others. This line of research is orthogonal to approaches that incorporate these constraint into the AD/AS methods, either directly or indirectly [4, 24, 53]. As a next step, one should perform an in-depth comparison of more constrained feature extractors here, and furthermore include rotation-equivariant feature extractors [12, 52] into said comparison (see Appendix A.4 for a motivation).

4.4. Data Augmentation

For this set of experiments, we set out to understand whether we could improve performance by augmenting our training set. We therefore artificially increased our training datasets by applying different sets of augmentations, implemented in the albumentations library [10]: (I) Affine transformations (rotation, scale and translation), (II) Blur, (III) RandomBrightnessContrast changes, (IV) Sharpening, and (V) Flipping (horizontal and vertical). Augmentations were carefully selected considering both prior work [21, 54] and the evaluated dataset, since flipping constitutes an anomaly for some categories of MVTEC AD (e.g. transistor) [41]. We therefore used the five augmentations outlined above for the VisA dataset, while restricting ourselves to the first four for the MVTEC AD dataset. For additional details about the augmentations' hyperparameters we refer to our code.

To now analyse the effect of the data augmentations, we disabled each respective augmentation in an ablation fashion, while keeping the remaining ones active. The number of augmentations was fixed across k-shots, and we augmented each training image 8 times, with only one type of augmentation being applied per augmented image. The

augmentation applied per image was furthermore randomly drawn from the set of all augmentations. Evaluations are moreover restricted to the few-shot regime (i.e. 1, 5 and 10 shots) due to VRAM limitations. We further constrained the feature extractor to the Anti-aliased WideResNet50 and the input scale to 2x, given that this hyperparameter combination provided the best performance in the previous set of tests and to reduce the computational cost of the evaluations.

Results: One can see in Tab. 3 that data augmentation can actually decrease performance on MVTEC AD. More specifically, we see that Sharpen seems to have an adverse effect on the achieved performance, since only its removal increases performance beyond the baseline. Repeating the experiment for the MVTEC AD dataset under the exclusion of the Sharpen augmentation further shows that only the combination of all augmentations outperforms the baseline (see Appendix A.3). On the contrary, for the VisA dataset, all assessed augmentation combinations outperform the baseline. Removing the Flip augmentation noticeably decreases the performance gain by a large margin, indicating that this augmentation is quite important for this dataset. We see that Affine, Blur and Sharpen do not seem to improve the performance of the system, given that the AUHPROC increases when these augmentations are removed. Furthermore, it is worth noting that BrightnessContrast augmentation does not seem to impact performance at all.

Overall, it seems that there is a benefit to be gained by using augmentations in the few to many-shot AD/AS settings. However, one is required to specifically tune the augmentations for each dataset to avoid accidentally decreasing performance. Note that this observation is in agreement with literature [61]. Moreover, performance boosts are much less pronounced compared to optimizing either feature extractor or input scale (see Tab. 2), and vary strongly between datasets (gain of 0.035 AUHPROC for VisA compared to 0.006 AUHPROC for MVTEC AD). We thus suggest that the former are optimized before investigating data augmentation techniques, and to employ data augmentation with care.

4.5. Coreset Subsampling and Data Augmentation

In the few-shot setting, using coreset in conjunction with data augmentation techniques might allow us to maintain performance improvements of the data augmentations while keeping the inference time low. We explore this possibility by applying a fixed number of augmentations to each k-shot while varying the coreset size. Specifically, we test applying 8 and 16 augmentations per training image, and vary the coreset size to be equal to that of 1, 4 or 8 images (corresponding to 3136, 12 544 and 25 088 points in the memory bank, respectively). We activated all the valid augmentations for the VisA dataset and the three augmenta-

Table 3. Influence of augmentations on few-shot performance. We disabled each respective augmentation while keeping the remaining ones active. We report the mean of category-wise AUHPROC generated after averaging over seeds/runs. We also report the relative gain/loss compared to the baseline of not augmenting. Best value per dataset are boldfaced. Abbreviations: # augs = number of augmentations, A = Affine, BC = BrightnessContrast, B = Blur, S = Sharpen, F = Flip.

	# augs	augmentation type					AUHPROC	
		A	BC	B	S	F	mean	diff
MVTec AD	0	x	x	x	x	x	67.6	0.0
	8	x	✓	✓	✓	x	67.1	-0.5
		✓	x	✓	✓	x	67.0	-0.6
			✓	x	✓	x	67.0	-0.6
				✓	x	x	68.2	0.6
					✓	x	66.8	-0.8
VisA	0	x	x	x	x	x	52.5	0.0
	8	x	✓	✓	✓	✓	56.0	3.5
		✓	x	✓	✓	✓	55.0	2.5
			✓	x	✓	✓	55.8	3.3
				✓	x	✓	55.5	3.0
					✓	x	53.7	1.2
				✓	55.0	2.5		

tions for MVTec AD that provided a benefit on the previous tests (Blur, BrightnessContrast and Affine). For direct comparability, we again used the Anti-aliased WideResNet50 as the feature extractor at 2x input scale. We furthermore again limit ourselves to the few-shot setting due to VRAM limitations.

Results: Table 4 shows that small coreset sizes are already sufficient to fully recapitulate the topology of the augmented training data. Specifically, complete recapitulation is realized at 4 images (12 544 points), since further increasing the coreset size does not further improve achieved performance. Moreover, further scaling the augmentation rate from 8 to 16 augmentations per image actually degrades achieved performance. This could indicate that there is some level of uncertainty/instability during greedy coreset selection when the ratio of true data to augmented data becomes too small. Alternatively, augmenting too much might skew the underlying training data distribution/topology.

Overall, coreset subsampling can be applied with a target coreset size of a few images, while augmenting the dataset, without decreasing the performance. Alternative coreset selection approaches such as bayesian coreset subsampling [32] might be investigated for a more stable as well as potentially faster coreset selection process in future work.

Table 4. Combining coreset subsampling with augmentations for few-shot AD/AS. We report mean and standard deviation of category-wise AUHPROC after averaging over seeds/runs. We use the Anti-aliased WideResNet50 as a feature extractor with an input scale of 2x. Best values per dataset are boldfaced.

	coreset size	# augmentations	AUHPROC	
			mean	std
MVTec AD	all	0	67.6	21.2
		8	68.2	20.3
	3136	8	68.1	20.4
		16	67.3	21.8
	12 544	8	68.2	20.3
		16	67.4	21.5
25 088	8	68.2	20.3	
	16	67.4	21.5	
VisA	all	0	52.5	20.0
		8	55.0	20.8
	3136	8	54.9	21.2
		16	54.6	20.5
	12 544	8	55.1	21.3
		16	54.7	20.5
25 088	8	55.1	21.3	
	16	54.7	20.5	

4.6. Comparison with the State of the Art

We continue by comparing the AD performance of PatchCore optimized for the few/many-shot regime with state-of-the-art few-shot AD methods. We focus on AD performance rather than on joint AD/AS performance to compare with as many methods as possible: While not all AD methods can be used for AS, AD outputs can be readily constructed for any AS method. Moreover, we evaluate on $k \in \{1, 2, 4\}$, since we found that most developed methods report AD performance for this set of k . To denote overall AD performance, we computed the arithmetic mean of the respective statistics over all values of k , i.e. weighting each shot equally. The optimal hyperparameters of PatchCore for the few-shot regime are as follows: (I) Feature extractor: Anti-aliased WideResNet50, (II) Input image size: 448×448 , (III) Number of augmentations per image: 8, (IV) Coreset size: 12 544.

Results: The optimized version of PatchCore depends the least on the samples selected for training on both MVTec AD and VisA, as denoted by its low standard deviations (Tab. 5). It moreover demonstrates favorable results on MVTec AD, achieving third place, and furthermore sets a new state of the art in AD on the more challenging

Table 5. Comparison with the state the art. We report the mean and standard deviation of AD performance over 5 random seeds each. Values for SPADE [15], PaDiM [18], and WinCLIP [27] are sourced from the WinCLIP paper [27], whereas values for GraphCore [53] and RegAD [24] are sourced from the respective papers. Best/second best value per dataset and k-shot are boldfaced/underlined respectively. "PCore ori" corresponds to anomalib's [2] reimplementaion of the PatchCore algorithm, using the default settings, whereas "PCore opt" corresponds to its optimized version.

		image-AUROC							
		1-shot		2-shot		4-shot		average	
method		mean	std	mean	std	mean	std	mean	std
MVTec AD	PCore opt	85.3	2.5	88.9	0.5	91.9	0.8	88.7	1.3
	PCore ori	81.8	1.1	86.4	2.2	89.5	1.7	85.9	1.7
	WinCLIP	93.1	<u>2.0</u>	94.4	<u>1.3</u>	95.2	<u>1.3</u>	94.2	<u>1.5</u>
	SPADE	81.0	<u>2.0</u>	82.9	2.6	84.8	2.5	82.9	2.4
	PaDiM	76.6	3.1	78.9	3.1	80.4	2.5	78.6	2.9
	RegAD	<u>89.9</u>	-	<u>91.9</u>	-	<u>92.9</u>	-	<u>91.6</u>	-
VisA	PCore opt	<u>83.6</u>	1.6	86.3	<u>1.2</u>	88.8	<u>0.7</u>	86.4	1.2
	PCore ori	<u>76.7</u>	<u>2.4</u>	80.0	0.9	83.2	0.6	80.0	<u>1.3</u>
	WinCLIP	83.8	4.0	<u>84.6</u>	2.4	<u>87.3</u>	1.8	<u>85.2</u>	2.7
	SPADE	79.5	4.0	<u>80.7</u>	5.0	81.7	3.4	<u>80.6</u>	4.1
	PaDiM	62.8	5.4	67.4	5.1	72.8	2.9	67.7	4.5

VisA dataset, where it is both the most consistent and most performant method. Also, both WinCLIP and GraphCore do not benefit as much from additional training data, as denoted by smaller increases in image-AUROC when increasing k (see also Fig. 1). For WinCLIP, this can be explained by the strong influence of language-guidance on the overall performance, as denoted by its impressive zero-shot results on MVTec AD [27]. Language-guidance is furthermore not used by WinCLIP currently when incorporating available training images in few/many-shot AD, and we believe this to be an avenue of future research. For GraphCore [53], we argue this is due to the strong biases incorporated in learning geometrically invariant feature representations. As a consequence, more training images bring only limited value, since only non-geometrical changes will be leveraged/learned by GraphCore.

Overall, this comparison validates our work, affirming that there is value in adapting pre-existing methods to few/many-shot AD/AS. Still, optimized Patchcore fails at times, and we provide an analysis of its failure cases in Appendix A.4.

4.7. Limitations

First, we did not optimize other AD/AS methods besides PatchCore, but plan to do so in future work. Due to compute constraints, we moreover did not ablate over the layer selection on the backbone. However, doing so on a per-category basis was shown to improve AD performance [22], and the optimal layers might furthermore depend on the number of shots k used. Next, we did not reimplement all methods in our comparison with the state of the art, but rather took the values from the corresponding sources directly. Unfortunately, most proposed methods do not provide reference implementations [27, 53], and we found some to be vague in their description [53], further increasing the difficulty of implementing them. Nonetheless, this should be done for a fair comparison, and we plan to do so in future work. Last, we did not perform a root-cause analysis on why anti-aliasing boosts AD/AS performance in the few/many-shot settings. We will therefore acquire a suitable dataset with higher variation in part positioning (i.e. translations, potentially also rotations) as a first step, rather than introducing these variations artificially (done e.g. in [4]). Afterwards, we will benchmark different constraints, i.e. translation and rotation-equivariant CNNs [12, 31, 52, 62], as well as their vision transformer counterparts [39, 55], on said dataset.

5. Conclusion

We performed a comprehensive study to optimize the various hyperparameters of PatchCore for the few/many-shot AD/AS settings. The study revealed that the feature extractor and the input resolution are the most important hyperparameters to tune. Additionally, we showed that image augmentations can be helpful, but need to be carefully designed using domain knowledge or one risks actually decreasing performance. Next, we showed that coreset subsampling combined with an adequate augmentation scheme allows one to keep inference times low while maintaining the benefits of augmenting the dataset. Combining all of this, we were able to achieve state-of-the-art AD performance on the challenging VisA dataset in the few-shot AD setting, demonstrating the merit of adapting pre-existing AD/AS methods to the few/many-shot settings. Finally, we showed that leveraging feature extractors with a stronger inductive bias such as anti-aliasing improves performance in the few/many-shot AD/AS settings, revealing a promising avenue for future research.

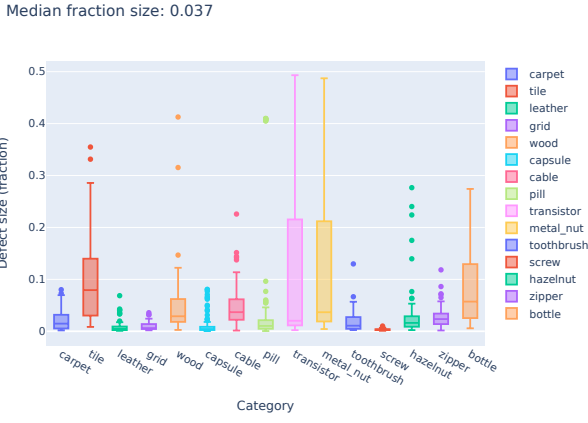
References

- [1] Pankaj Agarwal, Sariel Har, Peled Kasturi, and R Varadarajan. Geometric approximation via coresets. *Combinatorial and Computational Geometry*, 52, 11 2004. 4

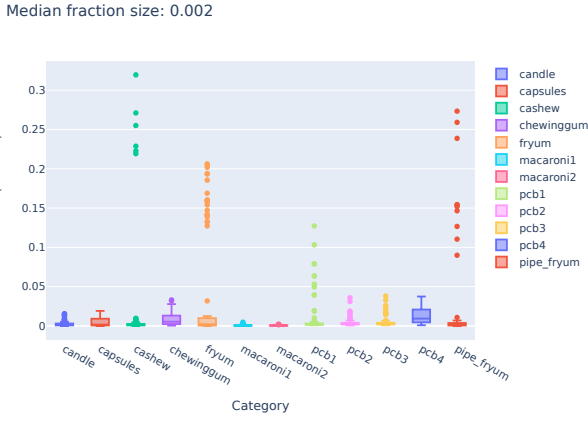
- [2] Samet Akcay, Dick Ameln, Ashwin Vaidya, Barath Lakshmanan, Nilesh Ahuja, and Utku Genc. Anomalib: A deep learning library for anomaly detection, 2022. 4, 8
- [3] Toshimichi Aota, Lloyd Teh Tzer Tong, and Takayuki Okatani. Zero-shot versus many-shot: Unsupervised texture anomaly detection. In *Proceedings of the IEEE/CVF Winter Conference on Applications of Computer Vision (WACV)*, pages 5564–5572, January 2023. 2
- [4] Aitor Artola, Yannis Kolodziej, Jean-Michel Morel, and Thibaud Ehret. Glad: A global-to-local anomaly detector. In *Proceedings of the IEEE/CVF Winter Conference on Applications of Computer Vision (WACV)*, pages 5501–5510, January 2023. 6, 8
- [5] Markus Bayer, Marc-André Kaufhold, and Christian Reuter. A survey on data augmentation for text classification. *ACM Computing Surveys*, 55(7):1–39, 2022. 3
- [6] Mikhail Belkin, Daniel Hsu, Siyuan Ma, and Soumik Mandal. Reconciling modern machine-learning practice and the classical bias–variance trade-off. *Proceedings of the National Academy of Sciences*, 116(32):15849–15854, 2019. 3
- [7] Paul Bergmann, Kilian Batzner, Michael Fauser, David Sattlegger, and Carsten Steger. The mvtec anomaly detection dataset: A comprehensive real-world dataset for unsupervised anomaly detection. *International Journal of Computer Vision*, Jan. 2021. 1, 3, 4
- [8] Paul Bergmann, Kilian Batzner, Michael Fauser, David Sattlegger, and Carsten Steger. Beyond dents and scratches: Logical constraints in unsupervised anomaly detection and localization. *International Journal of Computer Vision*, 2022. 5
- [9] Paul Bergmann, Michael Fauser, David Sattlegger, and Carsten Steger. MVTEC AD – a comprehensive real-world dataset for unsupervised anomaly detection. In *The IEEE Conference on Computer Vision and Pattern Recognition (CVPR)*, June 2019. 1, 3, 4
- [10] Alexander Buslaev, Vladimir I. Iglovikov, Eugene Khvedchenya, Alex Parinov, Mikhail Druzhinin, and Alexandr A. Kalinin. Albumentations: Fast and flexible image augmentations. *Information*, 11(2), 2020. 6
- [11] Yunkang Cao, Xiaohao Xu, Chen Sun, Yuqi Cheng, Zongwei Du, Liang Gao, and Weiming Shen. Segment any anomaly without training via hybrid prompt regularization, 2023. 2
- [12] Gabriele Cesa, Leon Lang, and Maurice Weiler. A program to build E(N)-equivariant steerable CNNs. In *International Conference on Learning Representations*, 2022. 6, 8, 13
- [13] Varun Chandola, Arindam Banerjee, and Vipin Kumar. Anomaly detection: A survey. *ACM computing surveys (CSUR)*, 41(3):1–58, 2009. 1
- [14] Xuhai Chen, Yue Han, and Jiangning Zhang. A zero-/few-shot anomaly classification and segmentation method for cvpr 2023 vand workshop challenge tracks 1&2: 1st place on zero-shot ad and 4th place on few-shot ad, 2023. 2
- [15] Niv Cohen and Yedid Hoshen. Sub-image anomaly detection with deep pyramid correspondences. *arXiv preprint arXiv:2005.02357*, 2020. 1, 8
- [16] Ekin D. Cubuk, Barret Zoph, Dandelion Mane, Vijay Vasudevan, and Quoc V. Le. Autoaugment: Learning augmentation strategies from data. In *Proceedings of the IEEE/CVF Conference on Computer Vision and Pattern Recognition*, pages 113–123, 2019. 3
- [17] Jesse Davis and Mark Goadrich. The relationship between precision-recall and roc curves. In *Proceedings of the 23rd international conference on Machine learning*, pages 233–240, 2006. 4
- [18] Thomas Defard, Aleksandr Setkov, Angélique Loesch, and Romaric Audigier. Padim: A patch distribution modeling framework for anomaly detection and localization. In Alberto Del Bimbo, Rita Cucchiara, Stan Sclaroff, Giovanni Maria Farinella, Tao Mei, Marco Bertini, Hugo Jair Escalante, and Roberto Vezzani, editors, *Pattern Recognition. ICPR International Workshops and Challenges*, pages 475–489, Cham, 2021. Springer International Publishing. 1, 4, 8
- [19] J. Deng, W. Dong, R. Socher, L. Li, Kai Li, and Li Fei-Fei. ImageNet: A large-scale hierarchical image database. In *2009 IEEE Conference on Computer Vision and Pattern Recognition*, pages 248–255, June 2009. 1, 3
- [20] Alexey Dosovitskiy, Lucas Beyer, Alexander Kolesnikov, Dirk Weissenborn, Xiaohua Zhai, Thomas Unterthiner, Mostafa Dehghani, Matthias Minderer, Georg Heigold, Sylvain Gelly, Jakob Uszkoreit, and Neil Houlsby. An image is worth 16x16 words: Transformers for image recognition at scale. In *International Conference on Learning Representations*, 2021. 3
- [21] Pierre Gutierrez, Antoine Cordier, Thaïs Caldeira, and Théophile Sautory. Data augmentation and pre-trained networks for extremely low data regimes unsupervised visual inspection. In *Automated Visual Inspection and Machine Vision IV*, volume 11787, page 1178703. SPIE, 2021. 3, 6
- [22] Lars Heckler, Rebecca König, and Paul Bergmann. Exploring the importance of pretrained feature extractors for unsupervised anomaly detection and localization. In *Proceedings of the IEEE/CVF Conference on Computer Vision and Pattern Recognition (CVPR) Workshops*, pages 2916–2925, June 2023. 3, 4, 5, 6, 8
- [23] Shell Xu Hu, Da Li, Jan Stühmer, Minyoung Kim, and Timothy M Hospedales. Pushing the limits of simple pipelines for few-shot learning: External data and fine-tuning make a difference. In *Proceedings of the IEEE/CVF Conference on Computer Vision and Pattern Recognition*, pages 9068–9077, 2022. 3
- [24] Chaoqin Huang, Haoyan Guan, Aofan Jiang, Ya Zhang, Michael Spratlin, and Yanfeng Wang. Registration based few-shot anomaly detection. In *European Conference on Computer Vision (ECCV)*, 2022. 2, 6, 8
- [25] Fabian Isensee, Paul F. Jaeger, Simon A. A. Kohl, Jens Petersen, and Klaus H. Maier-Hein. nnu-net: a self-configuring method for deep learning-based biomedical image segmentation. *Nature Methods*, 18(2):203–211, 2021. 2
- [26] Gareth James, Daniela Witten, Trevor Hastie, and Robert Tibshirani. *An Introduction to Statistical Learning: With Applications in R*. Springer Publishing Company, Incorporated, 2014. 3
- [27] Jongheon Jeong, Yang Zou, Taewan Kim, Dongqing Zhang, Avinash Ravichandran, and Onkar Dabeer. Winclip: Zero-

- /few-shot anomaly classification and segmentation. In *CVPR 2023*, 2023. [2](#), [4](#), [8](#)
- [28] Simon Kornblith, Jonathon Shlens, and Quoc V Le. Do better imagenet models transfer better? In *Proceedings of the IEEE/CVF Conference on Computer Vision and Pattern Recognition*, pages 2661–2671, 2019. [3](#), [6](#)
- [29] Ze Liu, Yutong Lin, Yue Cao, Han Hu, Yixuan Wei, Zheng Zhang, Stephen Lin, and Baining Guo. Swin transformer: Hierarchical vision transformer using shifted windows. In *Proceedings of the IEEE/CVF international conference on computer vision*, pages 10012–10022, 2021. [3](#)
- [30] Zhuang Liu, Hanzi Mao, Chao-Yuan Wu, Christoph Feichtenhofer, Trevor Darrell, and Saining Xie. A convnet for the 2020s. *Proceedings of the IEEE/CVF Conference on Computer Vision and Pattern Recognition (CVPR)*, 2022. [3](#), [4](#)
- [31] Hagay Michaeli, Tomer Michaeli, and Daniel Soudry. Alias-free convnets: Fractional shift invariance via polynomial activations. In *Proceedings of the IEEE/CVF Conference on Computer Vision and Pattern Recognition (CVPR)*, pages 16333–16342, June 2023. [8](#)
- [32] Cian Naik, Judith Rousseau, and Trevor Campbell. Fast bayesian coresets via subsampling and quasi-newton refinement. In S. Koyejo, S. Mohamed, A. Agarwal, D. Belgrave, K. Cho, and A. Oh, editors, *Advances in Neural Information Processing Systems*, volume 35, pages 70–83. Curran Associates, Inc., 2022. [4](#), [7](#)
- [33] Tiago S Nazare, Rodrigo F de Mello, and Moacir A Ponti. Are pre-trained CNNs good feature extractors for anomaly detection in surveillance videos? *arXiv preprint arXiv:1811.08495*, 2018. [1](#)
- [34] Avital Oliver, Augustus Odena, Colin Raffel, Ekin D. Cubuk, and Ian J. Goodfellow. Realistic evaluation of deep semi-supervised learning algorithms. In *Proceedings of the 32nd International Conference on Neural Information Processing Systems, NIPS’18*, pages 3239–3250, Red Hook, NY, USA, 2018. Curran Associates Inc. [2](#)
- [35] Yassine Ouali, Celine Hudelot, and Myriam Tami. Semi-supervised semantic segmentation with cross-consistency training. In *Proceedings of the IEEE/CVF Conference on Computer Vision and Pattern Recognition (CVPR)*, June 2020. [3](#)
- [36] Luis Perez and Jason Wang. The effectiveness of data augmentation in image classification using deep learning. *arXiv preprint arXiv:1712.04621*, 2017. [3](#)
- [37] Marco AF Pimentel, David A Clifton, Lei Clifton, and Lionel Tarassenko. A review of novelty detection. *Signal Processing*, 99:215–249, 2014. [1](#)
- [38] Foster Provost and Tom Fawcett. Analysis and visualization of classifier performance with nonuniform class and cost distributions. In *Proceedings of AAAI-97 Workshop on AI Approaches to Fraud Detection & Risk Management*, pages 57–63, 1997. [4](#)
- [39] Shengju Qian, Hao Shao, Yi Zhu, Mu Li, and Jiaya Jia. Blending anti-aliasing into vision transformer. In M. Ranzato, A. Beygelzimer, Y. Dauphin, P.S. Liang, and J. Wortman Vaughan, editors, *Advances in Neural Information Processing Systems*, volume 34, pages 5416–5429. Curran Associates, Inc., 2021. [8](#)
- [40] Oliver Rippel, Patrick Mertens, Eike König, and Dorit Merhof. Gaussian anomaly detection by modeling the distribution of normal data in pretrained deep features. *IEEE Transactions on Instrumentation and Measurement*, 70:1–13, 2021. [1](#), [2](#), [3](#)
- [41] Oliver Rippel, Patrick Mertens, and Dorit Merhof. Modeling the distribution of normal data in pre-trained deep features for anomaly detection. In *2020 25th International Conference on Pattern Recognition (ICPR)*, pages 6726–6733, 2021. [4](#), [6](#)
- [42] Karsten Roth, Latha Pemula, Joaquin Zepeda, Bernhard Schölkopf, Thomas Brox, and Peter Gehler. Towards total recall in industrial anomaly detection. In *Proceedings of the IEEE/CVF Conference on Computer Vision and Pattern Recognition (CVPR)*, pages 14318–14328, June 2022. [1](#), [2](#), [3](#), [4](#), [5](#)
- [43] Marco Rudolph, Bastian Wandt, and Bodo Rosenhahn. Same same but different: Semi-supervised defect detection with normalizing flows. In *Winter Conference on Applications of Computer Vision (WACV)*, Jan. 2021. [1](#), [2](#)
- [44] L. Ruff, J. R. Kauffmann, R. A. Vandermeulen, G. Montavon, W. Samek, M. Kloft, T. G. Dietterich, and K. R. Müller. A unifying review of deep and shallow anomaly detection. *Proceedings of the IEEE*, pages 1–40, 2021. [1](#), [5](#)
- [45] Thomas Schlegl, Philipp Seeböck, Sebastian M Waldstein, Georg Langs, and Ursula Schmidt-Erfurth. f-AnoGAN: Fast unsupervised anomaly detection with generative adversarial networks. *Medical image analysis*, 54:30–44, 2019. [1](#), [2](#)
- [46] Shelly Sheynin, Sagie Benaim, and Lior Wolf. A hierarchical transformation-discriminating generative model for few shot anomaly detection. In *Proceedings of the IEEE/CVF International Conference on Computer Vision*, pages 8495–8504, 2021. [2](#)
- [47] Mingxing Tan and Quoc Le. Efficientnetv2: Smaller models and faster training. In Marina Meila and Tong Zhang, editors, *Proceedings of the 38th International Conference on Machine Learning*, volume 139 of *Proceedings of Machine Learning Research*, pages 10096–10106. PMLR, 18–24 Jul 2021. [3](#)
- [48] Mingxing Tan and Quoc V. Le. EfficientNet: Rethinking model scaling for convolutional neural networks. In Kamalika Chaudhuri and Ruslan Salakhutdinov, editors, *Proceedings of the 36th International Conference on Machine Learning, ICML 2019, 9-15 June 2019, Long Beach, California, USA*, volume 97 of *Proceedings of Machine Learning Research*, pages 6105–6114. PMLR, 2019. [3](#), [4](#)
- [49] Hugo Touvron, Andrea Vedaldi, Matthijs Douze, and Hervé Jégou. Fixing the train-test resolution discrepancy. *Advances in neural information processing systems*, 32, 2019. [3](#)
- [50] Yulin Wang, Gao Huang, Shiji Song, Xuran Pan, Yitong Xia, and Cheng Wu. Regularizing deep networks with semantic data augmentation. *IEEE Transactions on Pattern Analysis and Machine Intelligence*, pages 1–1, 2021. [3](#)
- [51] Shengyun Wei, Shun Zou, Feifan Liao, and weimin lang. A Comparison on Data Augmentation Methods Based on Deep Learning for Audio Classification. In *Journal of Physics*

- Conference Series*, volume 1453 of *Journal of Physics Conference Series*, page 012085, Jan. 2020. 3
- [52] Maurice Weiler, Fred A. Hamprecht, and Martin Storath. Learning steerable filters for rotation equivariant cnns. In *2018 IEEE/CVF Conference on Computer Vision and Pattern Recognition*, pages 849–858, 2018. 6, 8, 13
- [53] Guoyang Xie, Jinbao Wang, Jiaqi Liu, Yaochu Jin, and Feng Zheng. Pushing the limits of fewshot anomaly detection in industry vision: Graphcore. In *The Eleventh International Conference on Learning Representations*, 2023. 2, 6, 8
- [54] Guoyang Xie, Jinbao Wang, Jiaqi Liu, Jiayi Lyu, Yong Liu, Chengjie Wang, Feng Zheng, and Yaochu Jin. Im-iad: Industrial image anomaly detection benchmark in manufacturing. *arXiv preprint arXiv:2301.13359*, 2023. 2, 3, 6
- [55] Renjun Xu, Kaifan Yang, Ke Liu, and Fengxiang He. \mathbb{S}^2 -equivariant vision transformer. In *The 39th Conference on Uncertainty in Artificial Intelligence*, 2023. 8
- [56] Jihun Yi and Sungroh Yoon. Patch svdd: Patch-level svdd for anomaly detection and segmentation. In *Proceedings of the Asian Conference on Computer Vision (ACCV)*, Nov. 2020. 1
- [57] Jason Yosinski, Jeff Clune, Anh Nguyen, Thomas Fuchs, and Hod Lipson. Understanding neural networks through deep visualization. *arXiv preprint arXiv:1506.06579*, 2015. 5
- [58] Sergey Zagoruyko and Nikos Komodakis. Wide residual networks. In *British Machine Vision Conference 2016*. British Machine Vision Association, 2016. 4
- [59] Vitjan Zavrtanik, Matej Kristan, and Danijel Skocaj. Draem - a discriminatively trained reconstruction embedding for surface anomaly detection. In *Proceedings of the IEEE/CVF International Conference on Computer Vision (ICCV)*, pages 8330–8339, Oct. 2021. 1
- [60] Vitjan Zavrtanik, Matej Kristan, and Danijel Skčaj. Reconstruction by inpainting for visual anomaly detection. *Pattern Recognition*, page 107706, 2020. 1
- [61] Lingrui Zhang, Shuheng Zhang, Guoyang Xie, Jiaqi Liu, Hua Yan, Jinbao Wang, Feng Zheng, and Yaochu Jin. What makes a good data augmentation for few-shot unsupervised image anomaly detection? In *Proceedings of the IEEE/CVF Conference on Computer Vision and Pattern Recognition (CVPR) Workshops*, pages 4344–4353, June 2023. 3, 6
- [62] Richard Zhang. Making convolutional networks shift-invariant again. In *International Conference on Machine Learning*, pages 7324–7334. PMLR, 2019. 3, 4, 8
- [63] Yang Zou, Jongheon Jeong, Latha Pemula, Dongqing Zhang, and Onkar Dabeer. Spot-the-difference self-supervised pre-training for anomaly detection and segmentation. *arXiv preprint arXiv:2207.14315*, 2022. 1, 2, 3, 4



(a)



(b)

Figure 3. Distribution of defect sizes for (a) MVTEC AD and (b) VisA.

A. Appendix

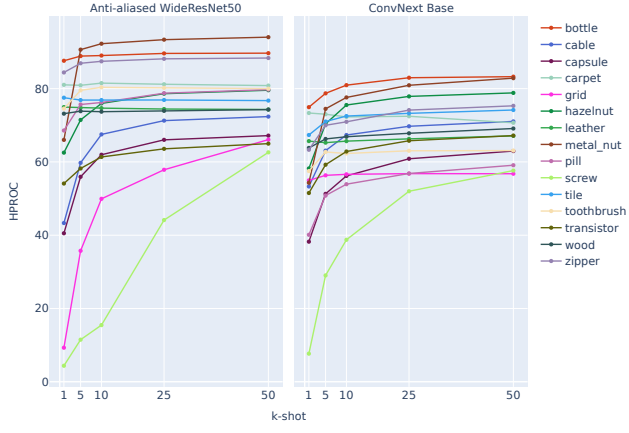
A.1. Defect Size

Figures 3a and 3b show the distribution of defect size as a fraction of the image’s pixels, for both MVTEC AD and VisA categories. One can see from these results that defects in VisA are generally much smaller than in MVTEC AD, which can partially explain its increased difficulty.

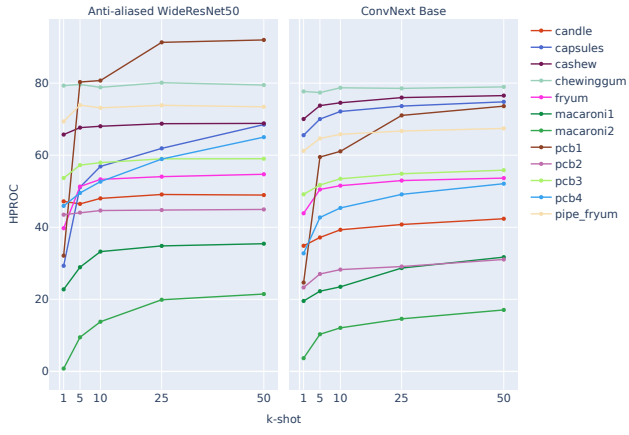
A.2. Influence of Dataset, Feature Extractor and Input Resolution

A.2.1 Influence of Dataset and Input Resolution

Table 6 shows the AUHPRC on both MVTEC AD and VisA. Looking more closely at this performance, we can see that the trend of increase in performance with an increase in scale is stronger in VisA compared to MVTEC AD. One may argue that this is due to the fact that VisA contains smaller defects than MVTEC AD, and that higher resolution might



(a)



(b)

Figure 4. HPROC across k-shots for (a) MVTEC AD and (b) VisA dataset, using Anti-aliased WideResNet50 (left) and ConvNext Base (right) as feature extractors at 2x their original input scale.

thus better facilitate their detection (see also Appendix A.1).

A.2.2 Influence of Feature Extractor and Dataset

We plot category-wise HPROC vs. k-shot curves for two different feature extractors (Anti-aliased WideResNet50 and ConvNext Base), at their best-performing scale (2x), in Figs. 4a and 4b. We see that even though the Anti-aliased WideResNet50 performs best overall, it does not perform best in all categories and shots (e.g. ”capsules” and ”cashew” of VisA).

A.2.3 Influence of Feature Extractor and Scale

We show in Fig. 5 the HPROC vs. k-shot curves for each backbone. Specifically, we compute the mean and standard deviation of HPROC across categories, scales and seed-/runs.

Table 6. Performance between different input scales on MVTec AD and VisA datasets. For each dataset, we report the mean of category-wise AUHPROC after averaging over feature extractors and seeds/runs. We also report the relative performance gain/loss between input scales 0.5x, 1.5x and 2.0x compared to the original input scale 1x.

input scale	AUHPROC						
	1.0x (original scale)	0.5x		1.5x		2.0x	
	mean	mean	diff	mean	diff	mean	diff
MVTec AD	63.3	52.1	-11.2	66.9	3.6	68.3	5.0
VisA	45.5	34.6	-10.9	50.2	4.7	53.0	7.5

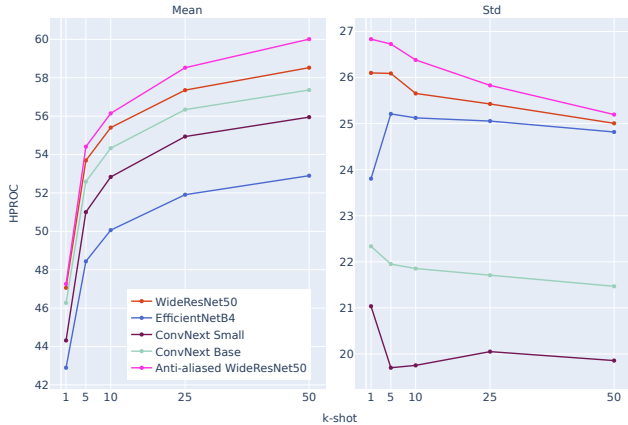


Figure 5. Mean and standard deviation of HPROC across k-shots for different feature extractors, averaged over datasets, input scales, and seeds/runs.

A.3. Data Augmentation

We further investigate the effect of augmentations on MVTec AD without using the Sharpen augmentation and only keep Affine, BrightnessContrast and Blur augmentations. We employ an Anti-aliased WideResNet50 at 2x its original scale. We can see in Tab. 7 that applying the three augmentations allows us to surpass the case where no augmentations are applied, and that disabling any one of the augmentations greatly decreases performance. This indicates that the combination of these three augmentations is important to actually increase performance.

A.4. Failure Case Analysis

We report category-wise image-AUROC scores of optimized PatchCore (see Sec. 4.6) for both MVTec AD and VisA across different k-shots to identify failure cases. Assessing Tab. 8, we see that certain categories where normal data contains strong rotations yield sub-optimal results (e.g. "screw" for MVTec AD and "macaroni2" on VisA, see Fig. 6 for some qualitative examples). It is worth noting here that CNNs are not rotation-equivariant by design. This can be attributed to the inherent properties of the con-

Table 7. Performance between different augmentation settings on MVTec AD dataset. We disabled each respective augmentation while keeping the remaining ones active. We report the mean of category-wise AUHPROC generated after averaging over seeds/runs. We also report the relative gain/loss of different augmentation combinations compared to disabling augmentation. Abbreviations: # augs = number of augmentations, A = Affine, BC = BrightnessContrast, B = Blur.

# augs	augmentation type			AUHPROC	
	A	BC	B	mean	diff
0	✗	✗	✗	67.6	0.0
8	✗	✓	✓	67.3	-0.3
	✓	✗	✓	67.4	-0.2
		✓	✗	67.2	-0.4
			✓	68.2	0.6

volution operation, which relies on fixed filters to extract local features. As a result, CNNs struggle to generalize across different rotation angles, leading to a decreased performance. Therefore, one should additionally investigate rotation-equivariant networks [12, 52] as pre-trained feature extractor in future work for further performance improvements.

Table 8. Category-wise image-AUROC scores of optimized PatchCore for MVTec AD and VisA across different k-shots. We report the mean and standard deviation over 5 random seeds for each category.

		image-AUROC									
		1-shot		2-shot		4-shot		5-shot		10-shot	
	category	mean	std	mean	std	mean	std	mean	std	mean	std
MVTec AD	bottle	99.4	0.4	99.3	0.4	99.4	0.3	99.8	0.3	99.7	0.4
	cable	71.7	6.1	77.3	3.6	84.2	8.4	82.9	3.3	87.0	3.6
	capsule	78.6	12.9	90.1	4.8	86.4	11.8	94.3	4.6	92.8	4.5
	carpet	97.0	0.5	97.4	0.6	97.2	0.2	97.2	0.4	97.5	0.7
	grid	65.5	6.4	74.1	3.5	86.0	5.9	90.2	4.8	93.7	3.8
	hazelnut	91.1	4.1	95.7	3.3	98.7	1.0	98.8	0.8	99.9	0.2
	leather	100.0	0.0	100.0	0.0	100.0	0.0	100.0	0.0	100.0	0.0
	metal-nut	79.0	2.4	88.0	5.6	90.7	5.1	97.0	0.8	99.1	0.6
	pill	83.1	2.3	85.5	2.0	87.6	1.5	89.7	2.5	91.0	1.8
	screw	49.2	2.8	53.6	4.5	59.4	3.9	62.1	3.7	70.5	4.9
	tile	99.0	0.8	98.8	1.1	98.8	0.5	98.9	0.4	98.9	0.3
	toothbrush	93.1	2.6	96.1	2.7	97.2	3.4	99.4	0.8	99.9	0.2
	transistor	76.6	14.6	81.4	13.3	95.1	0.3	95.0	0.5	96.4	0.2
	wood	99.5	0.1	99.4	0.2	99.5	0.2	99.4	0.1	99.5	0.1
zipper	96.2	1.6	97.5	2.2	98.9	0.4	98.9	0.8	99.2	0.2	
VisA	candle	93.4	1.4	93.5	1.0	93.6	1.3	93.6	0.6	95.0	1.0
	capsules	64.2	6.8	66.3	4.1	70.1	3.6	70.3	1.8	76.2	1.7
	cashew	93.7	1.4	95.3	1.2	96.7	0.6	96.8	0.7	96.6	0.7
	chewinggum	97.8	0.5	97.7	0.2	98.4	0.5	97.9	0.3	97.9	0.5
	fryum	84.1	1.2	80.1	4.3	89.1	2.4	92.0	1.6	93.2	1.1
	macaroni1	75.6	3.2	80.7	4.6	86.4	2.9	87.3	5.7	92.3	2.2
	macaroni2	58.9	8.8	59.4	4.8	61.2	3.1	64.3	7.8	66.7	2.5
	pcb1	80.3	19.5	90.5	3.7	93.1	3.8	94.7	2.4	96.8	0.9
	pcb2	88.5	1.6	91.3	0.6	92.9	0.8	92.3	0.9	93.4	0.8
	pcb3	83.0	2.3	85.9	2.0	88.3	1.4	90.3	2.5	91.8	1.4
	pcb4	86.5	11.0	96.2	2.1	97.0	2.3	98.5	1.1	98.7	0.4
	pipe-fryum	97.6	1.3	98.8	0.3	99.0	0.1	99.2	0.2	99.3	0.1

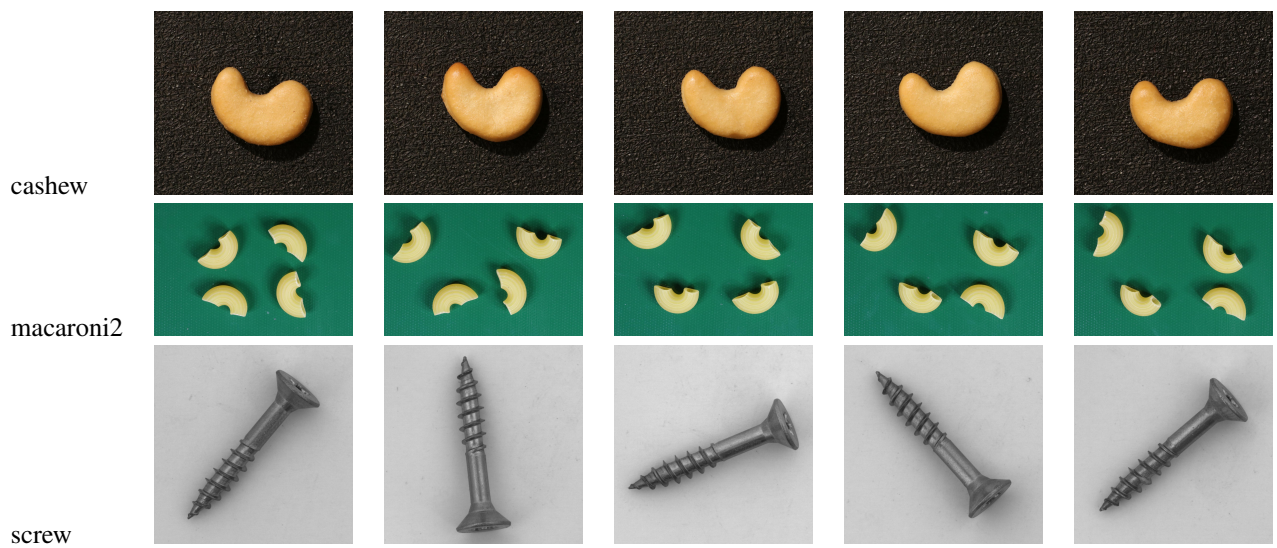


Figure 6. Low degree of rotation for "cashew" compared to high degree of rotation for "macaroni2" and "screw".